Fabrication of Different SnO2 Nanorods for Enhanced Photocatalytic Degradation and Antibacterial Activity

Govindhan Gnanamoorthy
University of Madras
Virendra Kumar Yadav
Jaipur National University
Krishna Yadav (envirokrishna@gmail.com)
Bundelkhand University Faculty of Science https://orcid.org/0000-0002-4228-2726
Kandasamy Ramar
Jamal Mohamed College
Javed Alam
King Saud University
Arun Kumar Shukla
King Saud University
Fekri Abdulraqeb Ahmed Ali
King Saud University
Mansour Alhoshan
King Saud University

Research Article

Keywords: Hydrothermal method, Acid-mediated, Malachite Green dye, Photocatalyst, Antibacterial

Posted Date: February 8th, 2021

DOI: https://doi.org/10.21203/rs.3.rs-157108/v1

Version of Record: A version of this preprint was published at Environmental Science and Pollution Research on April 10th, 2021. See the published version at https://doi.org/10.1007/s11356-021-13627-w.

Abstract

The acid-mediated (Oxalic acid [OXA], Cinnamic acid [CA], and itaconic acid [IA]) SnO_2 nanorods were synthesized by the hydrothermal method. The synthesized SnO_2 nanorods, in turn, were analyzed with various physic-chemical techniques such as the X-Ray Diffraction (XRD), Fourier Transform Infrared Spectroscopy (FT-IR), scanning electron microscope (SEM), and Raman spectroscopy. Furthermore, the photocatalytic activity of the different SnO_2 nanorods was investigated with the malachite green (MG) dye under visible light illumination. The OXA-SnO_2 nanorods displayed an excellent degradation performance with observed values of 91% compared to other nanomaterials' (CA and IA-SnO_2) photocatalytic activity. The different synthesized SnO_2 materials were tested for antibacterial and antifungal studies; this result may be used or developed in future research activities.

1. Introduction

A novel nanomaterial have most attractive and considered due to the photocatalytic applications. recently, food and pharmaceuticals, textile, leather, and paper industries reported materials contains several organic aromatic groups and molecules are produced toxic gas and other moieties, which is highly damage in an environment (Bouras et al. 2019). However, these dyes are highly toxic and affect human, animal, and bird health disorders and damaging ecosystems (Gruzeł et al. 2019). Nowadays, pollution can be controlled with soluble dyes and used in various fields in the emerging world. For instance, Sirajul (2019) reported that the Cd ions incorporated into the SnO_2 nanoparticles are favoured for the absorption process and thermodynamic studies. Meanwhile, the researchers developed SnO_2 based nanomaterials for several applications such as in electrochemical sensors, solar cells, battery studies, fuel cells, supercapacitors, biological studies and photocatalytic activities (Chen et al. 2019; Dilip and Jayaprakash 2018; Honarmand et al. 2019; Mao et al. 2019; Liu 2019; Saravanakumar et al. 2019; Singh et al. 2019; Sousa et al. 2019; Tammina et al. 2019; Wang et al. 2019). In case some people used different toxic chemicals and synthesis methods, it has been explained by the morphology and band gap energy. Therefore, the photocatalytic activity of different acid-mediated SnO_2 nanorods was tested.

Moreover, several metal oxides are currently reported to be used in the field of photocatalysis, such as ZnS based materials, WO_3, (Sn(IV)/TiO_2/AC), Ag/ZnO, $ZnSn(OH)_6$, N-doped ZnS, PVDF/TiO_2 nanofibers, 3D g-C_3N_4, β-Bi_2O_3@Bi_2S_3, BiOCl nanocubes, MoS_2@Fe_3O_4, and rGO/$CdWO_4$. However, these types of materials, created for the first time, displayed a better efficiency in photocatalytic performances with a well-known photo-generated recombination used in different light sources with respect to the various organic pollutants and dyes. These semiconductor materials possess more favorable photocatalytic studies boosting the degradation efficiency as well as exhibiting the synergistic effects (Dong et al. 2017; Yu et al. 2018; Sun et al. 2018; Cai et al. 2019; Sun et al. 2006; Tie et al. 2018; Tan et al. 2018; Tie et al. 2019; Zhang et al. 2017; Tie et al. 2019; Heo et al. 2019; Dong et al. 2019a; Dong et al. 2019b).

This study aims to introduce the SnO_2 nanorods which have a tetragonal crystal system with the materials having been characterized by the surface morphology and various physic-chemical methods. The SnO_2 nanorod has a few advantages including being facile, eco-friendly, easily available, having mild reactions and reduced toxicity, and lower costs of the synthesized materials. The synthesized OXA, CA, and IA-SnO_2 nanomaterials were used for the photocatalytic studies under the visible light source with the malachite green dye. However, the OXA-SnO_2 nanomaterials gained a higher efficiency when compared with the CA and IA-SnO_2 nanomaterials.

2. Materials And Methods

2.1. Materials

The number of standard chemicals required for the material synthesis was the recommended analytical grade chemicals, such as stannous chloride ($SnCl_2.2H_2O$), Oxalic acid ($C_2H_2O_4$), Cinnamic acid ($C_9H_8O_2$), and Itaconic acid ($C_5H_6O_4$), with NaOH materials with Methanol and Ethanol used as solvents.

2.2. Synthesis of SnO_2 nanorods

The SnO_2 nanorods were first synthesized by the hydrothermal method. In a typical procedure, 1 mm of the $SnCl_2.2H_2O$ was dissolved in methanol, making three sets with each set of the solution added dropwise in different acids such as oxalic acid, cinnamic acid, and itaconic acid. These precursors were stirring for 1 hour, then, the liquid NaOH (0.1M) was added and the solution stirred overnight for 12 hours. The obtained homogeneous solution was then transferred to the stainless-steel autoclave, maintaining the temperature at 180 °C. The obtained product was washed with ethanol and water several times, followed by drying at a vacuum oven at 25 °C overnight.

2.3. Antibacterial studies

The antibacterial activity of the SnO_2 nanorods was evaluated for the different pathogens by using the agar well diffusion method (Gnanamoorthy et al. 2020). This bacterial analysis was performed by the antibiotic condition. The synthesized SnO_2 nanorod was tested to the *Staphylococcus aureus* (Gram-positive), *Escherichia coli* (Gram-negative), *Pseudomonas aeruginosa* (Gram-negative), *Candida albicans* (Antifungal), and *Enterococcus faecalis* bacteria (Gram-positive)—all cultured from the Mueller-Hinton agar with incubated temperatures at 32–35 °C for 48 hours. The 0.9% saline solution was used for washing with observed bacterial strain intensity OD values for 0.5 at 571 nm, and then different higher concentrations (100 µg/mL, 200 µg/mL, and 500 µg/mL) were added in the well and different positive controls (20 µg/mL) (*S. Aureus*, *E. Faecalis* – Amoxicillin, *E. Coli, P. Aeruginosa* – Levofloxacin, *C. Albicans* – Fluconazole) were used, after being measured for the zone of inhibition.

2.4. Characterization

The three different synthesized SnO_2 nanomaterials were characterized and confirmed by XRD (Rigaku, Dmax-2500) with the surface morphology images captured by SEM (Hitachi, S-4800). The phase orientation confirmation was recorded by FT-IR and Raman spectroscopy (WQF-410 and LABRAM-HR system with laser excitation of 514.5 nm). The dye degradation studies were carried out by UV-Visible spectroscopy (Hitachi U-3010). The photocatalytic measurement was recorded by the photocatalytic reactor (Techinstro).

3. Results And Discussion

3.1. Structural analysis

The three different SnO_2 nanorods were synthesized by the hydrothermal method. Fig.1 (a-c) shows the XRD patterns of the synthesized materials and observed all the diffraction Bragg peak positions compared to the reference and well-matched with JCPDS card no 10–1854. The sharp peaks seem to assemble SnO_2 nanorods with different acids' sample methods. The obtained diffraction peaks at 26.0°, 33.9°, 38.1°, 51.8°, 54.2°, 57.9°, 61.9°, 64.7°, 65.9°, 71.3°, and 78.6° corresponding to the (110), (101), (200), (211), (220), (002), (120), (112), (301), (250), and (321) planes. The synthesized SnO_2 nanorods were identified the tetragonal system in all three samples. The CA and IA-SnO_2 samples obtained for the lower intensity had some differences when compared to the OXA-SnO_2 nanorods. These three acid-mediated SnO_2 nanorods showed diffraction peaks without shifting 2θ values than the lattice parameter which also increased. The OXA, CA, and IA-SnO_2 nanorods crystallite size were calculated by the Debye-Scherrer formula (Eqn-1),

$$D = K\lambda / \beta \cos\theta \qquad 1$$

Here, K is the shape factor, λ the wavelength, and θ the diffraction angle. The evaluated crystallite size is in decreasing order of the materials, OXA-SnO_2 > CA-SnO_2 >IA-SnO_2 nanomaterials, 38 nm, 37 nm, and 32 nm, respectively.

3.2. FT-IR spectroscopy

The chemical composition of the three different synthesized SnO_2 nanorods was characterized by the FT-IR spectroscopy method. The SnO_2 nanorods' FT-IR comparison spectra is shown in Fig. 2 (a-c) and evaluated by the several vibration peaks. The vibration peak at 400–620 cm^{-1} corresponds to the O-Sn-O and Sn-O stretching vibrations which is similar to the previously reported work (Ali et al. 2019; Chen et al. 2012). The peak 1608 cm^{-1} is attributed to the bending vibration modes of the N-H group and 3340 cm^{-1} can be ascribed to the O-H stretching or N-H stretching vibrations of absorbed water molecules (Liu et al. 2019). The CA-SnO_2 nanoparticles' vibration peak transmittance has been decreased depending on the formation of molecules. Hence, synthesized SnO_2 functional groups were confirmed and the results coincide with the Raman spectroscopy. Therefore, the materials' functional groups were confirmed, which has been used for the subsequent application process.

3.3. Raman spectroscopy

Fig. 3 (a-c) shows the Raman spectra of the OXA, CA, and IA-SnO_2 nanorods, the three peaks appeared with good agreement results. The overall characteristic peaks are at 240, 472, and 627 cm^{-1} which are associated with the A_1g vibration mode at 625 cm^{-1}. The peak 240 and 472 cm^{-1} are the Eg vibration modes of different SnO_2 nanorods (Hui Liu et al. 2019). The other peak at 240 cm^{-1} is the companion peak associated with the vibration $\upsilon 1^c(A_1^c)$ of the edge-sharing of the SnO_2 structure.

3.4. DRS UV-Visible spectroscopy

The OXA, CA, and IA-SnO_2 nanorods' diffuse reflectance spectroscopy results were shown in Fig. 4 (a-c). The SnO_2 nanorods were synthesized at a temperature of 180°C and the optical band gap energy was evaluated using the Kubelka-Munk equation (given below Eqn-2).

$$\alpha h\upsilon = A(h\upsilon - E_g)^{\eta} \qquad 2$$

Where α is the proportionality constant, A the absorption coefficient, hυ the Planck constant, and Eg the band gap respectively. The obtained DRS-UV results show that the OXA, CA, and IA-SnO_2 nanorods have identified red shift regions of the transition. The OXA, CA, and IA-SnO_2 nanoparticles' band gap energies were at 2.5 eV, 2.8 eV, and 3.0 eV, while preparing the low band gap energy compared to the reported band gap values (Chen 2019 et al.; Kar et al. 2019). The OXA-SnO_2 nanoparticles exhibited lower band gap energies when compared to the CA and IA-SnO_2 materials. As a result, all these SnO_2 nanomaterials were used to enhance the photocatalytic performances.

3.5. Morphology studies

Fig. 5 (a-d) shows the scanning electron microscope images of OXA-SnO_2 and these images explained by the nanorod like structure with bundles of rods edge-to-edge carefully merging with each other and obtained with a diameter range of 3-1 μm. The CA-SnO_2 surface morphology is shown in Fig. 6 (a-d), the synthesized material has shown layers like structure with diameter range is 1μm. The IA-SnO_2 surface morphology is shown in Fig. 7 (a-d) and the morphology illustrated that the tube tablet-like structure with a diameter range of 300 to 500 nm. All the synthesized SnO_2 nanomaterials were confirmed by various techniques and have shown low band gap energy, therefore, the photocatalytic activity should be enhanced.

3.6. Photocatalytic activity

Fig. 8-10 (a-d) explains that the absorption spectra of the MG photodegradation in the presence of different SnO_2 nanorods showed a maximum absorption range at 630 nm. Fig. 8-10 (a) shows the evidence of the photocatalyst dye degradations of the MG under visible light illumination of 500 nm, Fig. 8-10 (b) displays the function of time (Ct/C_0) and the photodegradation with respect to concentration and

the reaction time. Fig. 8-10 (c) illustrates the calculated degradation percentage, here the OXA-SnO_2 nanorods have been shown an excellent degradation compared to other mediated SnO_2 nanomaterials, the kinetic first order scan rate was calculated and the value found to be R^2-0.997, 0.997, and 0.988 and the slope value 0.0299, 0.0184, and 0.034 for OXA-SnO_2, CA-SnO_2 and IA-SnO_2 respectively. However, the intensity of the adsorption peak decreased within 90, 60, and 50 minutes, the monitored degradation (Fig. 8-10 (d)) process percentages at 91, 78, and 66. Summarized, the synthesized different SnO_2 nanorods evaluated an excellent photocatalytic performance under the visible light source.

The obtained degradation efficiency of the SnO_2 nanomaterials such as OXA-SnO_2 and CA-SnO_2 nanoparticles are 78% and 66%, the results of which show low degradation efficiency with electron transfer when compared to the OXA-SnO_2 due to it having low bandgap energy. This band gap energy plays a key role in the formation of desirable defects of suitable photocatalytic behavior. In the presence of visible light, the acid-mediated SnO_2 nanomaterials produced charge recombination barriers in the valance and conduction bands. For the conduction band, the whole pair of H_2O/OH^- interacted with the Hydroxyl ($OH^•$) in a radical formation, the conduction band of O_2 produced to the $O_2^{•-}$ and $HO_2^•$ were converted to H_2O_2 and $OH^•$ formation which strongly separates the radical formation. The detailed mechanism has been displayed in Fig.11.

Therefore, the above experimental results suggest that the synthesized SnO_2 nanomaterial was enhanced to the photocatalytic dye degradation and the OXA-SnO_2 nanorods have enhanced the photocatalytic activity when compared to other reported materials (Kaviyarasu et al. 2016).

3.7. Antibacterial and antifungal activities

SnO_2 nanoparticles were analyzed for antibacterial and antifungal activities, which corresponds to the *Staphylococcus aureus* (Gram-positive), *Escherichia coli* (Gram-negative), *Pseudomonas aeruginosa* (Gram-negative), *Candida albicans* (Antifungal), and *Enterococcus faecalis* bacteria (Gram-positive) zones of inhibition shown in Fig. 12 (a-e). Here, the first three bacteria (*Staphylococcus aureus* (Gram-positive), *Escherichia coli* (Gram-negative), *Pseudomonas aeruginosa* (Gram-negative) have higher antibacterial activity due to the particle size and Sn^{2+} ions (Hada et al. 2018). The *Candida albicans* (Antifungal) and *Enterococcus faecalis* bacteria (Gram-positive) are not inhibited by the activity (Table-1). Among them, the strains were tested only for higher concentrations, as the lower concentration did not support the activity. Therefore, this SnO_2 material was enhancing antibacterial and antifungal activities.

Table 1. Antibacterial activity against different pathogens with positive controls of Amoxicillin, Levofloxacin, Fluconazole.

S. No	Pathogens	1mg/mL	2mg/mL	5mg/mL	Positive Control	Negative Control
1	S. Aureus	28	30	32	32	-
2	E. Coli	28	28	30	34	-
3	*P. Aeruginosa*	25	27	32	38	-
4	*C. Albicans*	-	-	-	-	-
5	*E. Faecalis*	-	-	-	-	-

*** Zone of inhibition: Concentration (20 µg/ml) used for different positive control.**

4. Conclusion

All three different SnO_2 nanorods were synthesized by the hydrothermal method. The prepared nanomaterial structure, functional groups, and the surface morphology were investigated and confirmed by the XRD, FT-IR, SEM, and Raman analysis. The XRD results confirmed the tetragonal structure of the SnO_2 nanorods and the metal oxide functional groups were identified and confirmed by the FT-IR analysis. Additionally, the samples showed nanorod like structures. All the obtained SnO_2 nanorods applied the photocatalytic performances with malachite green dye. The synthesized SnO_2 nanomaterials enhanced the degradation; meanwhile, the OXA-SnO_2 nanorods displayed an excellent photocatalytic performance when compared to the other materials. The OXA-SnO_2 nanomaterials enhanced the antibacterial activity.

Declarations

Ethical Approval

Not applicable

Consent to Participate

Not applicable

Consent to Publish

Not applicable

Authors Contributions

Govindhan Gnanamoorthy: Conceptualization, Methodology, Writing- Original Draft, Writing- Review and Editing. **Virendra Kumar Yadav:** Data Curation, Writing- Original Draft, Review and Editing**. Krishna Kumar Yadav:** Resources, Writing- Original Draft, Writing- Review and Editing. **Kandasamy Ramar:** Writing- Original Draft, Review and Editing. **Javed Alam:** Project Administrator, Resources, Writing- Review and Editing. **Arun Kumar Shukla:** Validation, Writing- Original Draft, Formal analysis. **Fekri Abdulraqeb Ahmed Ali**: Formal analysis, Writing- Original Draft, Review and Editing. **Mansour Alhoshan:** Writing- Original Draft, Writing- Review and Editing.

Funding

The authors extend their appreciation to the Deputyship for Research & Innovation, “Ministry of Education” in Saudi Arabia for funding this research work through the project number IFKSURG-1439-085.

Competing Interests

The authors declare that they have no known competing financial interests or personal relationships that could have appeared to influence the work reported in this paper.

Availability of data and materials

Data sharing not applicable to this article as no datasets were generated or analyzed during the current study.

Conflict of interest

The authors declare no conflict of interest.

Acknowledgment

The authors are indebted to the Department of Inorganic Chemistry, University of Madras, Guindy Campus, Chennai, for all the valuable support and needful facilities.

References

Bouras K, Slaoui A (2019) Photon management properties of Yb-doped SnO_2 nanoparticles synthesized by sol-gel technique, Physical Chemistry Chemical Physics, 1-24.

Chen Z (2019) Fabrication and characterization of polypyrrole coatings by embedding antimony modified SnO_2 nanoparticles, Journal of Industrial and Engineering Chemistry.

Cai J, Huang J, Wang S, Iocozzia J, Sun Z, Sun J, Yang Y, Lai Y, Lin Z (2019) Crafting Mussel-Inspired Metal Nanoparticle-Decorated Ultrathin Graphitic Carbon Nitride for the Degradation of Chemical

Pollutants and Production of Chemical Resources, Advanced Materials, 1806314.

Chen S, Liu F, Xu M, Yan J, Zhang F, Zhao W, Zhang Z, Deng Z, Yun J, Chen R, Liu C (2019) First-principles calculations and experimental investigation on SnO_2@ZnO heterojunction photocatalyst with enhanced photocatalytic Performance, Journal of Colloid and Interface Science, 553: 613–621.

Chen H, Ding L, Sun W, Jiang Q, Hu J, Li L (2015) Synthesis and Characterization of Ni Doped SnO_2 Microspheres with Enhanced Visible-light Photocatalytic Activity, RSC Advances, **5:** 56401-56409.

Dong S, Xia L, Zhang F, Li F, Wang Y, Cui L, Feng J, Sun J (2019) Effects of pH value and hydrothermal treatment on the microstructure and natural-sunlight photocatalytic performance of $ZnSn(OH)_6$ photocatalyst, Journal of Alloys and Compounds 810:151955.

Dong S, Cui L, Zhang W, Xia L, Zhou S, Russell C K, Fan M, Feng J, Sun J (2019) Double-shelled $ZnSnO_3$ hollow cubes for efficient photocatalytic degradation of antibiotic wastewater, Chemical Engineering Journal, 123279.

Dilip R, Jayaprakash R (2018) Synthesis and characterization of $BaFe_2O_4$ nano-ferrites for gas sensor applications, Energy, Ecology and Environment, 3: 237–241.

Dong C, Fu Y, Zang W, He H, Xing L, Xue X (2017) Self-powering/self-cleaning electronic-skin basing on PVDF/TiO_2 nanofibers for actively detecting body motion and degrading organic pollutants, Applied Surface Science, 416: 424-431.

Ghoreishian S M, Seeta Rama Raju G, Pavitra E, Kwak C H, Han Y K, Yun Suk Huh (2019) Ultrasound-assisted heterogeneous degradation of tetracycline over flowerlike rGO/$CdWO_4$ hierarchical structures as robust solar-light-responsive photocatalysts: Optimization, kinetics, and mechanism, Applied Surface Science 489: 110–122.

Gruzeł G (2019) Preparation of Pt-skin PtRhNi Nanoframes Decorated with Small SnO_2 nanoparticles as an Efficient Catalyst for Ethanol Oxidation Reaction, ACS Appl. Mater. Interfaces 11:22352–22363.

Gnanamoorthy G, Virendra Kumar Yadav, Narayanan V (2020) Well organized assembly of (X)- $CuSnO_3$ nanoparticles enhanced photocatalytic and anti-bacterial properties. Journal of Water Process Engineering 36, 101258.

Heo N S, Shukla S (2019) Shape-controlled assemblies of graphitic carbon nitride polymer for efficient sterilization therapies of water microbial contamination via 2D g-C_3N_4 under visible light illumination, Materials Science & Engineering C, 104: 109846.

Honarmand M (2019) Biosynthesis of tin oxide (SnO_2) nanoparticles using jujube fruit for photocatalytic degradation of organic dyes, Advanced Powder Technology 30:1551–1557.

Liu H (2017) Cu nanoparticles/Fluorine-Doped Tin Oxide (FTO) Nanocomposites for Photocatalytic H_2 Evolution under Visible Light Irradiation, Catalysts 7:385.

Kumar Tammina S, Kumar Mandal B, Nawaz Khan F (2018) Mineralization of toxic industrial dyes by gallic acid mediated synthesized photocatalyst SnO_2 nanoparticles, Environmental Technology & Innovation 1-37.

Kar A, Olszowka J, Sain S et.al (2019) Morphological effects on the photocatalytic properties of SnO_2 Nanostructures, Journal of Alloys and Compounds, 810: 151718.

Kaviyarasu K, John Kennedy, Manikandan E, Mohamed Henini, Maaza Malik (2016) Photodegradation of organic pollutants RhB dye using UV simulated sunlight on ceria based TiO_2 nanomaterials for antibacterial Applications, Scientific Reports, 6: 38064.

Liu D, Pan J (2019) Ag decorated SnO_2 nanoparticles to enhance formaldehyde sensing Properties, Journal of Physics and Chemistry of Solids 124:36–43.

Mao Y , Tian Q (2019) Improving the lithium storage performance of SnO_2 nanoparticles by in-situ embedding into a porous carbon framework, Journal of Alloys and Compounds 803:224-230.

Magdalane C.M, Kaviyarasu K, Matinise N, Mayedwa N, Mongwaketsi N, Letsholathebe D, Mola G.T, Abdullah Al-Dhabi N, Arasu M.V, Henini M, Kennedy J, Maaza M, Jeyaraj B (2018) Evaluation on La_2O_3 garlanded ceria heterostructured binary metal oxide nanoplates for UV/ Visible light induced removal of organic dye from urban wastewater, South African Journal of Chemical Engineering, 26: 49-60.

Magdalane C.M, Kaviyarasu K, Raja A, Arularasu M.V, Genene T. Mola, Abdulgalim B. Isaev, Naif Abdullah Al-Dhabi, Mariadhas Valan Arasu, Jeyaraj B, Kennedy J, Maaza M (2018) Photocatalytic decomposition effect of erbium doped cerium oxide nanostructures driven by visible light irradiation: Investigation of cytotoxicity, antibacterial growth inhibition using catalyst. Journal of Photochemistry and Photobiology B: Biology, 185: 275-282.

Naif Mohammed Al-Hada, Halimah Mohamed Kamari, Anwar Ali Baqer, Abdul H. Shaari, Elias Saion (2018) Thermal Calcination-Based Production of SnO2 Nanopowder: An Analysis of SnO_2 Nanoparticle Characteristics and Antibacterial Activities. Nanomaterials, 8, 250.

Sun J, Wang X, Sun J, Sun R, Sun S, Qiao L (2006) Photocatalytic degradation and kinetics of Orange G using nano-sized Sn(IV)/TiO_2/AC photocatalyst, Journal of Molecular Catalysis A: Chemical, 260: 241–246.

Sun J, Cai Y, Xu H, Zou Z, Hu M, Jin X, Sun L, Li D, Xia D (2018) Synthesis of porous BiOCl nanocubes with enhanced visible light photocatalytic performance, Chemical Physics Letters, 711: 207-212

Saravanakumar B, Ravi G, Ganesh V (2019) Low Surface Energy and pH Effect on SnO_2 nanoparticles Formation for Supercapacitor Applications Journal of Nanoscience and Nanotechnology, 19: 3429–3436.

Sirajul H (2019) Adsorption of Cd^{2+} ions onto SnO_2 nanoparticles synthesized via sol-gel method: physiochemical study, Mater. Res. Express 6: 105035.

Sousa C A (2019) Metal (loid) oxide (Al_2O_3, Mn_3O_4, SiO_2 and SnO_2) nanoparticles cause cytotoxicity in yeast via intracellular generation of reactive oxygen species Applied Microbiology and Biotechnology 103:6257–6269.

Tie L, Sun R, Jiang H , Liu Y, Xia Y, Li Y, Chen H,Yu C, Dong S, Sun J, Sun J (2019) Facile fabrication of N-doped ZnS nanomaterials for efficient photocatalytic performance of organic pollutant removal and H_2 production, Journal of Alloys and Compounds, 807:151670.

Tan L, Yu C, Wang M, Zhang S, Sun J, Dong S, Sun J, (2018) Synergistic effect of adsorption and photocatalysis of 3D g-C_3N_4-agar hybrid aerogels, Applied Surface Science, 467–468: 286-292.

Tie L, Yang S, Yu C, Chen H, Liu Y, Dong S, Sun J, Sun J (2019) In situ decoration of ZnS nanoparticles with Ti_3C_2 MXene nanosheets for efficient photocatalytic hydrogen evolution, Journal of Colloid and Interface Science, 545: 63-70.

Tie L, Yu C, Zhao Y, Chen H, Yang S, Sun J, Dong S, Sun J (2018) Fabrication of WO_3 nanorods on reduced graphene oxide sheets with augmented visible light photocatalytic activity for efficient mineralization of dye, Journal of Alloys and Compounds, 769: 83-91.

Vikram Singh A (2019) Peptide-Induced Biomineralization of Tin Oxide (SnO_2) nanoparticles for Antibacterial Applications, Journal of Nanoscience and Nanotechnology,19: 5674–5686,

Wang Q (2018) Large-scale carbon framework microbelts anchoring ultrafine SnO_2 nanoparticles with enhanced lithium storage properties, Electrochimica Acta,297: 879-887.

Wang Q, Dong S, Zhang D, Yu C, Lu J, Wang D, Sun J (2017) Magnetically recyclable visible-light-responsive MoS_2@Fe_3O_4 photocatalysts targeting efficient wastewater treatment, Journal of Materials Science, 53: 1135–1147

Yu C, Yang P, Tie L, Yang S, Dong S, Sun J, Sun J (2018) One-pot fabrication of β-Bi_2O_3@Bi_2S_3 hierarchical hollow spheres with advanced sunlight photocatalytic RhB oxidation and Cr(VI) reduction activities, Applied Surface Science . 455: 8-17

Zhang L, Zhu D, He H, Wang Q, Xing L, Xue X (2017) Enhanced piezo/solar-photocatalytic activity of Ag/ZnO nanotetrapods arising from the coupling of surface plasmon resonance and piezophototronic effect, Journal of Physics and Chemistry of Solids 102: 27–33.

Figures

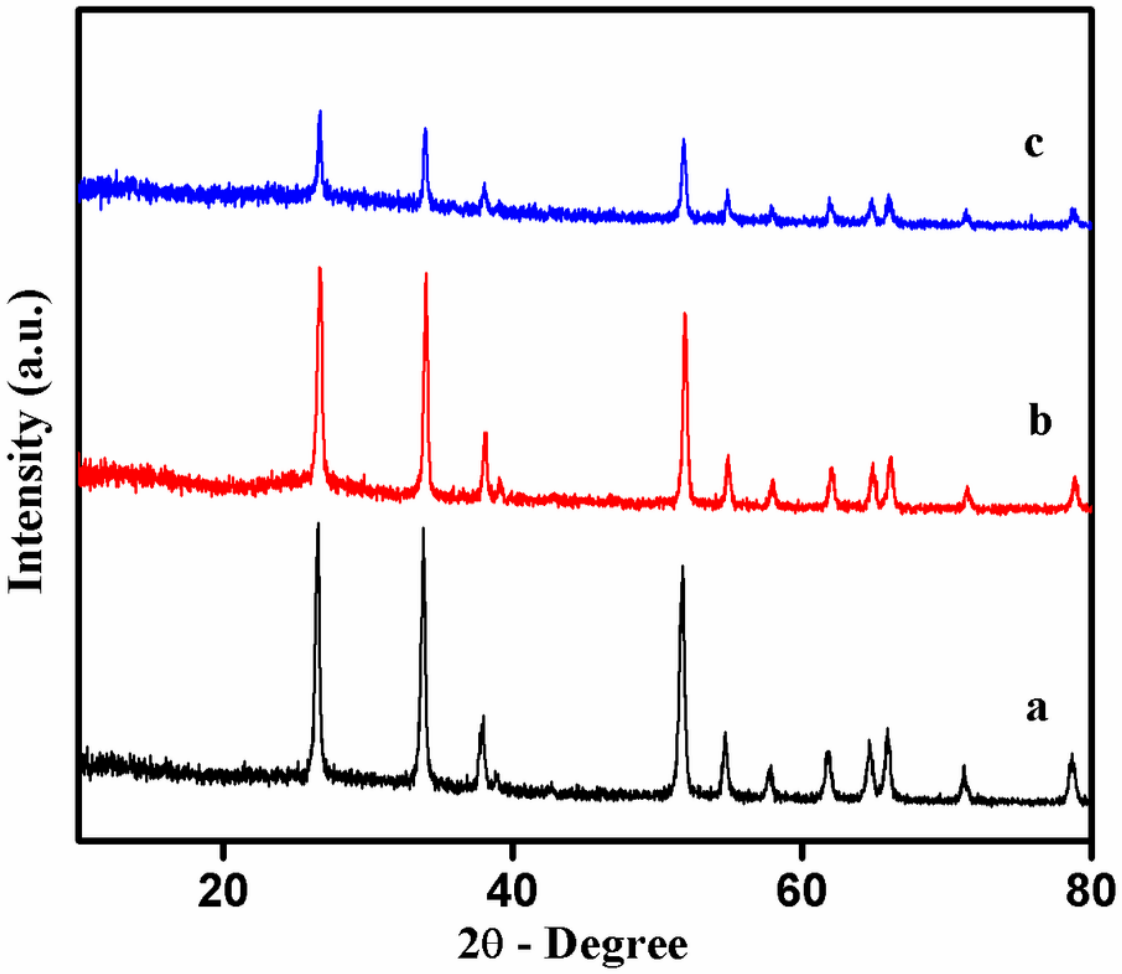

Figure 1

(a-c) XRD patterns of (a) OXA, (b) CA, and (c) IA-SnO2 nanorods.

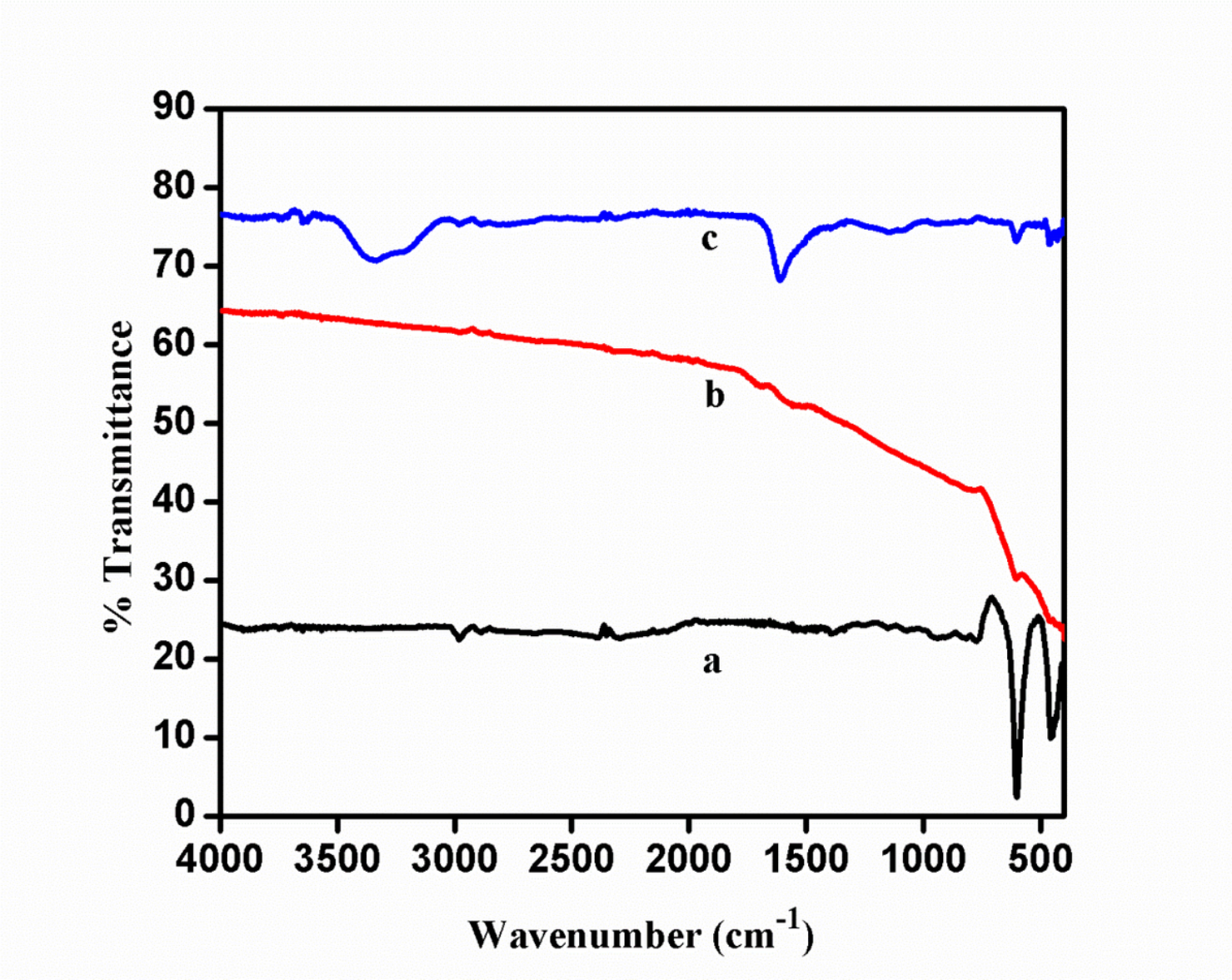

Figure 2

(a-c) FT-IR spectra of (a) OXA, (b) CA and (c) IA-SnO2 nanorods.

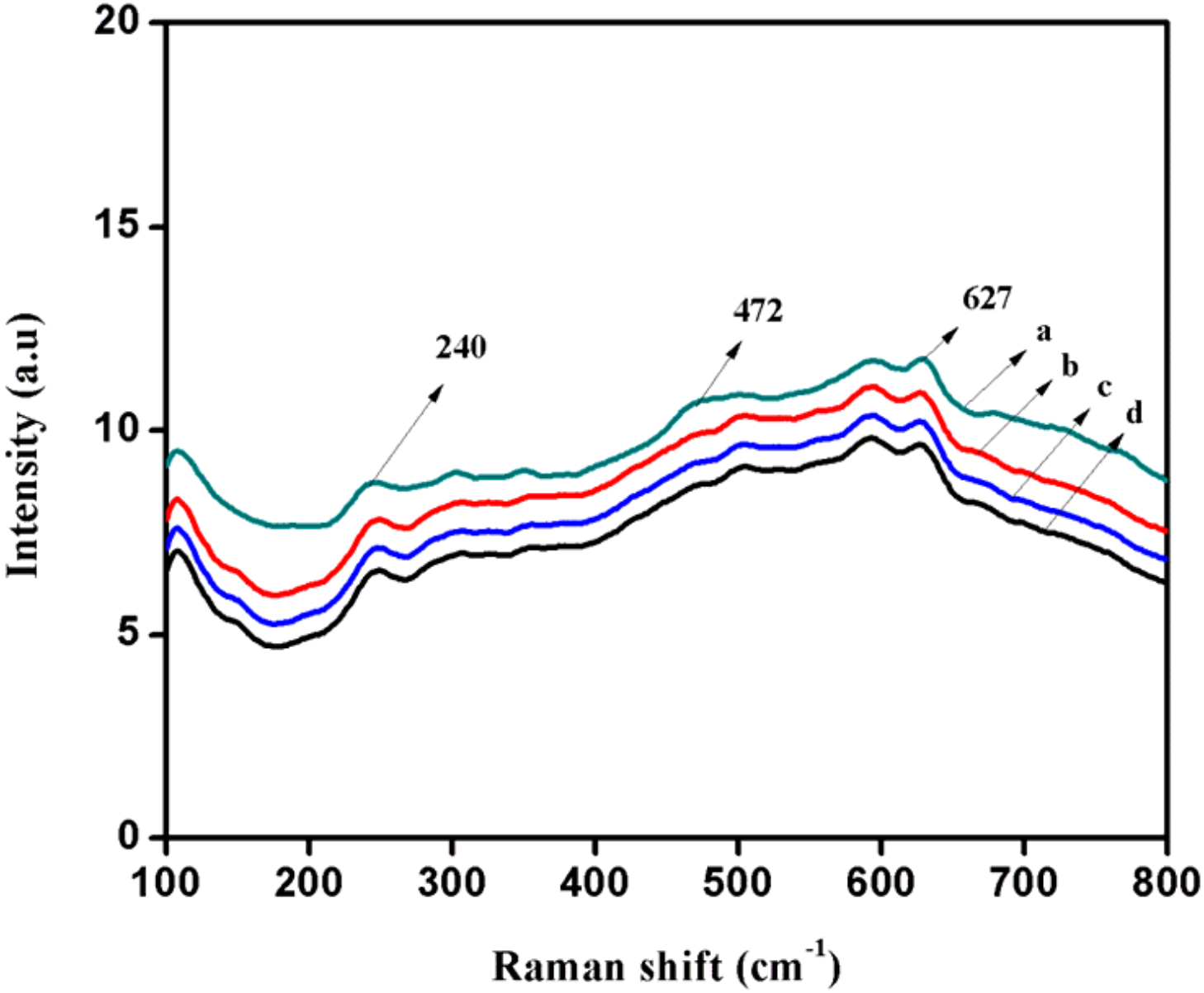

Figure 3

(a-c) Raman spectra of (a) OXA, (b) CA and (c) IA-SnO2 nanorods.

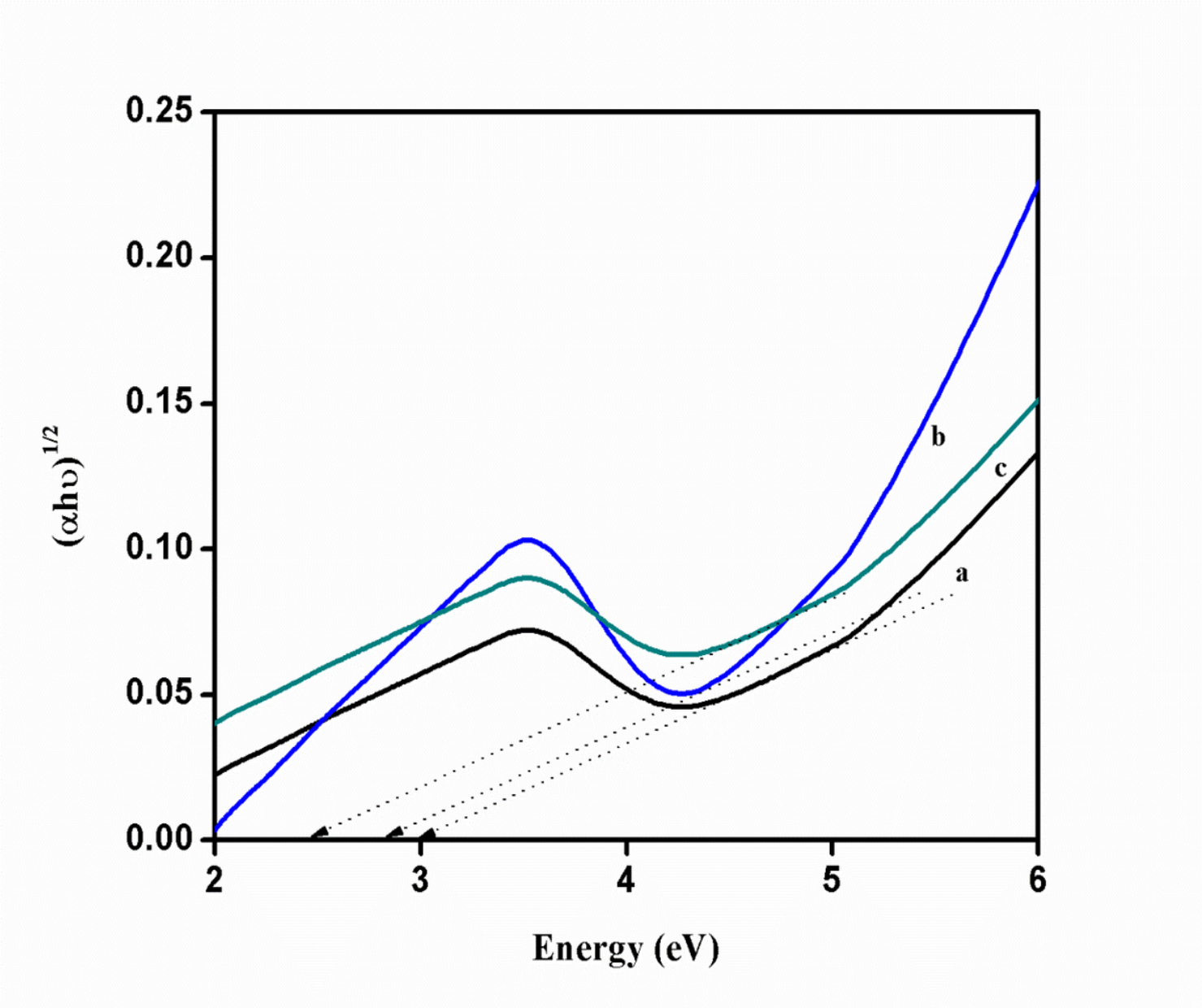

Figure 4

(a-c) Band gap energy of acid mediated (a) IA, (b) CA and (c) OXA-SnO2 nanorods.

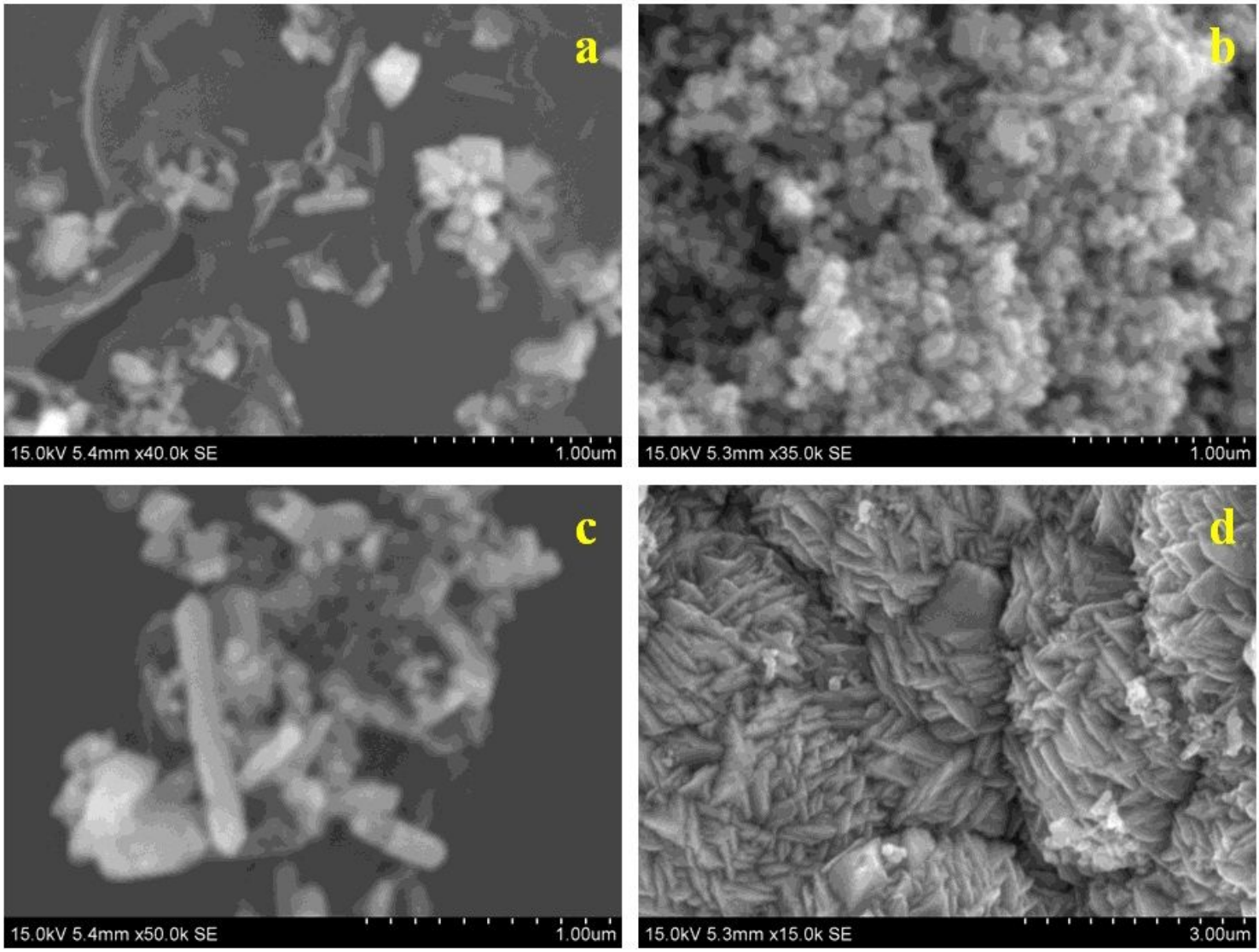

Figure 5

(a-d) SEM images of OXA-SnO2 nanorods.

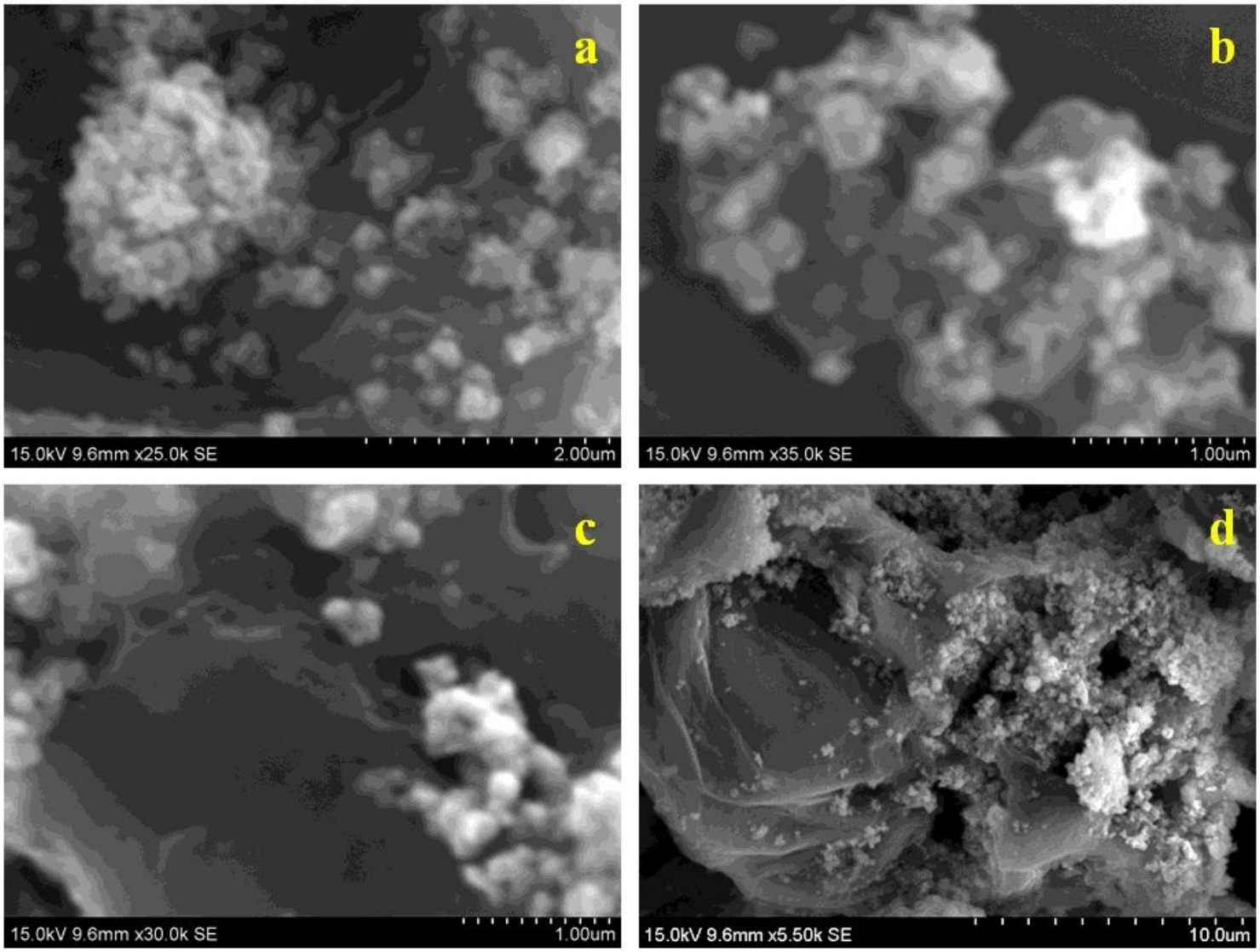

Figure 6

(a-d) SEM images of CA-SnO2 nanorods.

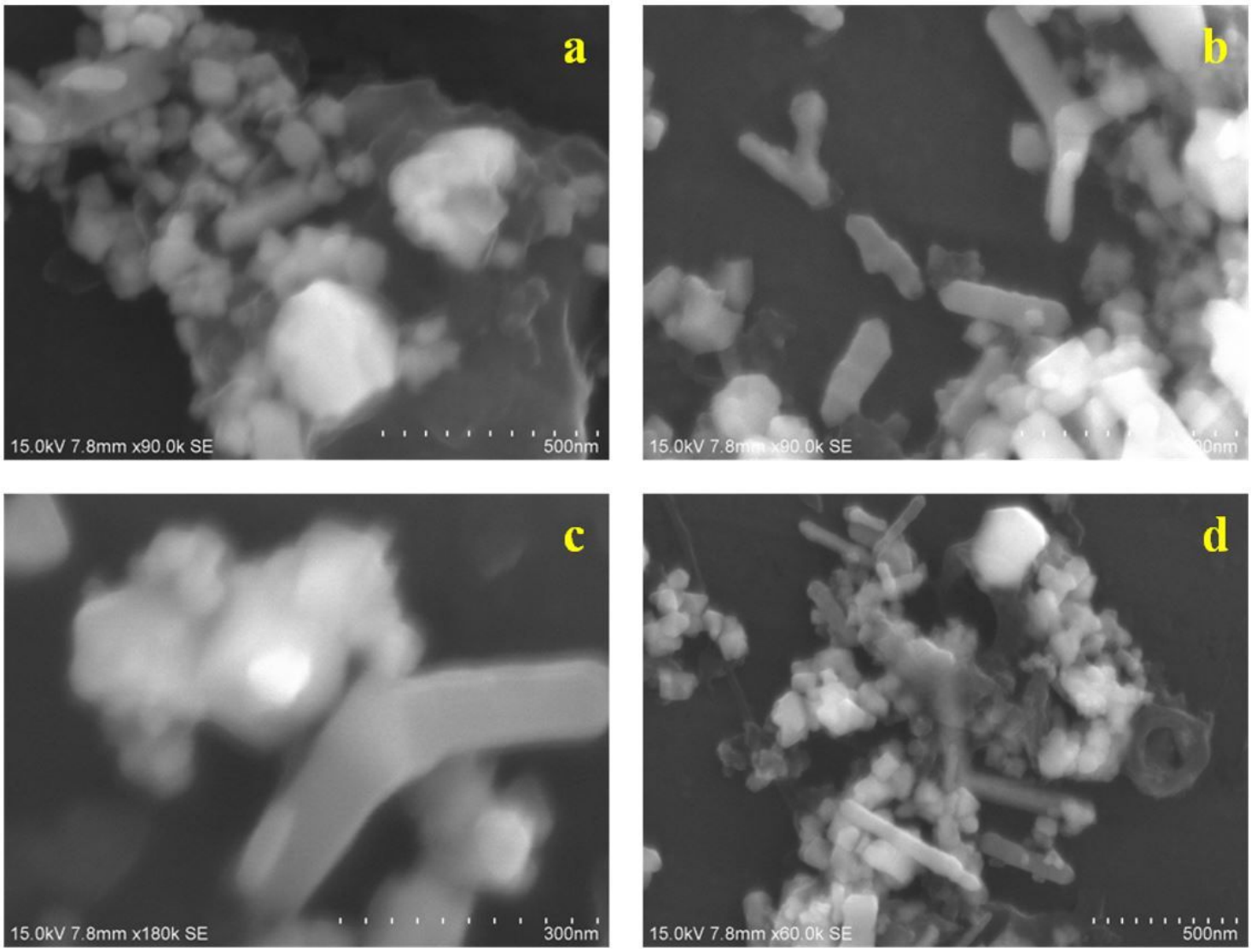

Figure 7

(a-d) SEM images of IA-SnO2 nanorods.

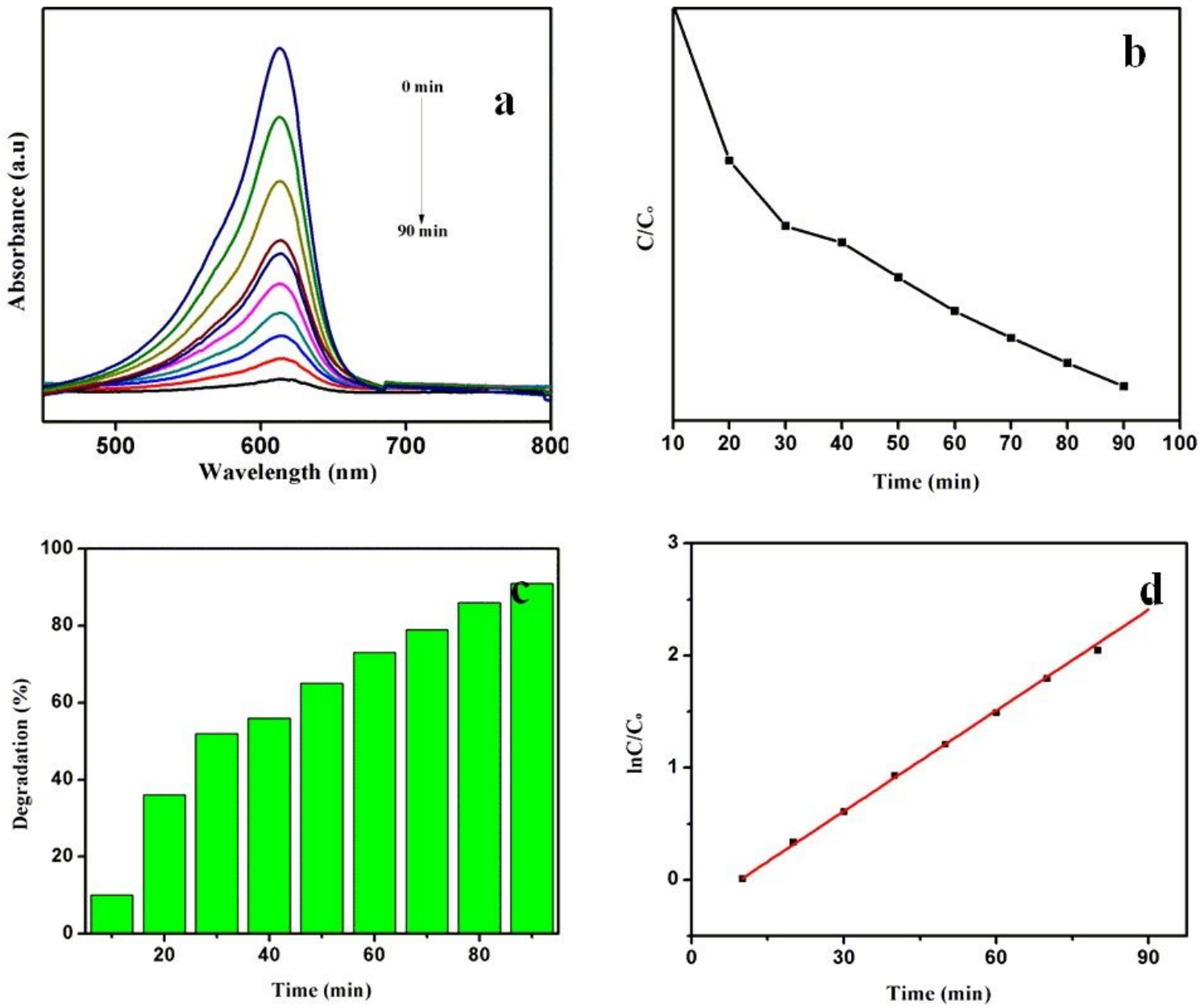

Figure 8

(a) Dye degradation (b) Concentration of C/Co (c) percentage of degradation and (d) Rate constant of OXA-SnO2 nanorods.

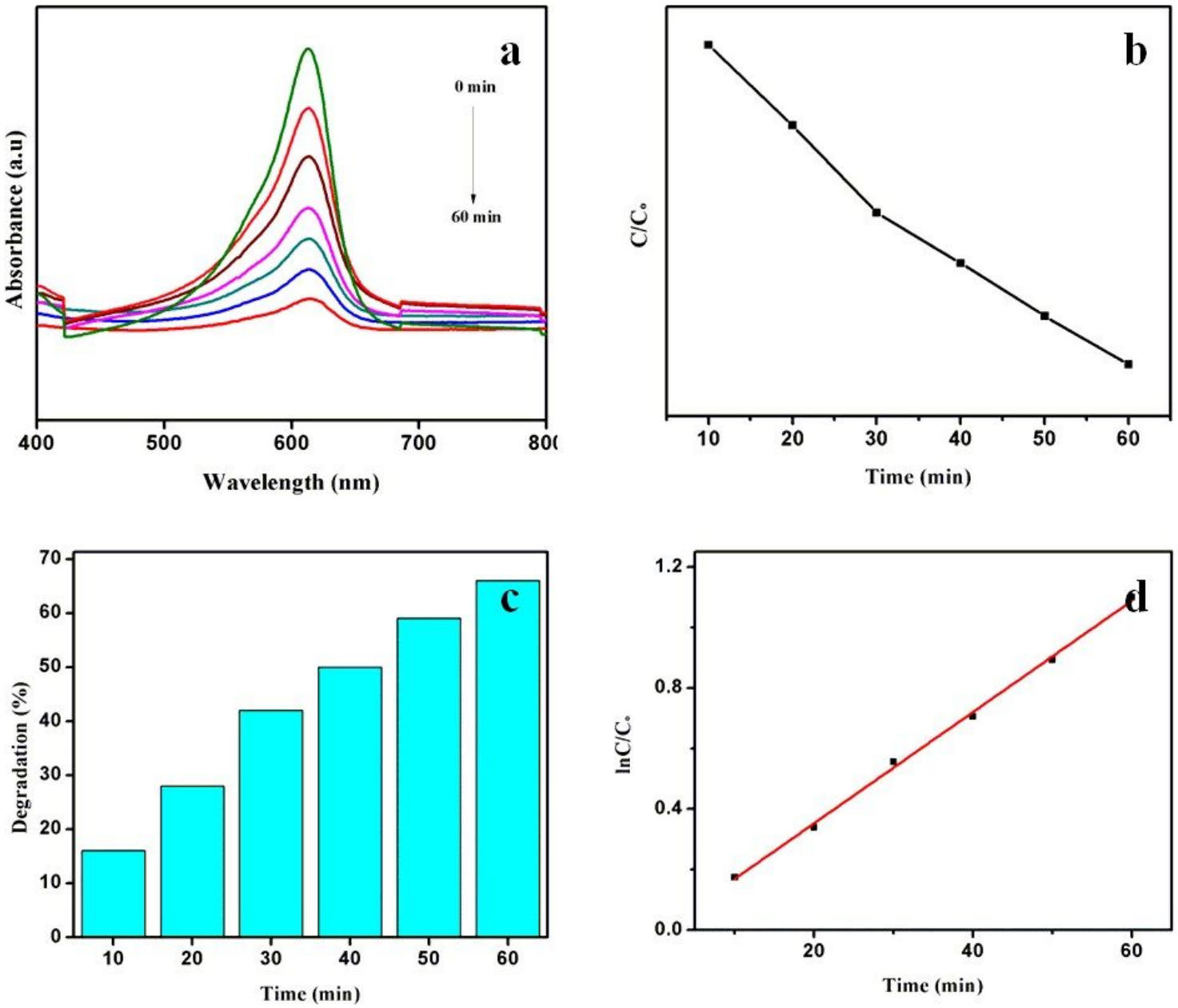

Figure 9

(a) Dye degradation (b) Concentration of C/Co (c) percentage of degradation and (d) Rate constant of CA-SnO2 nanorods.

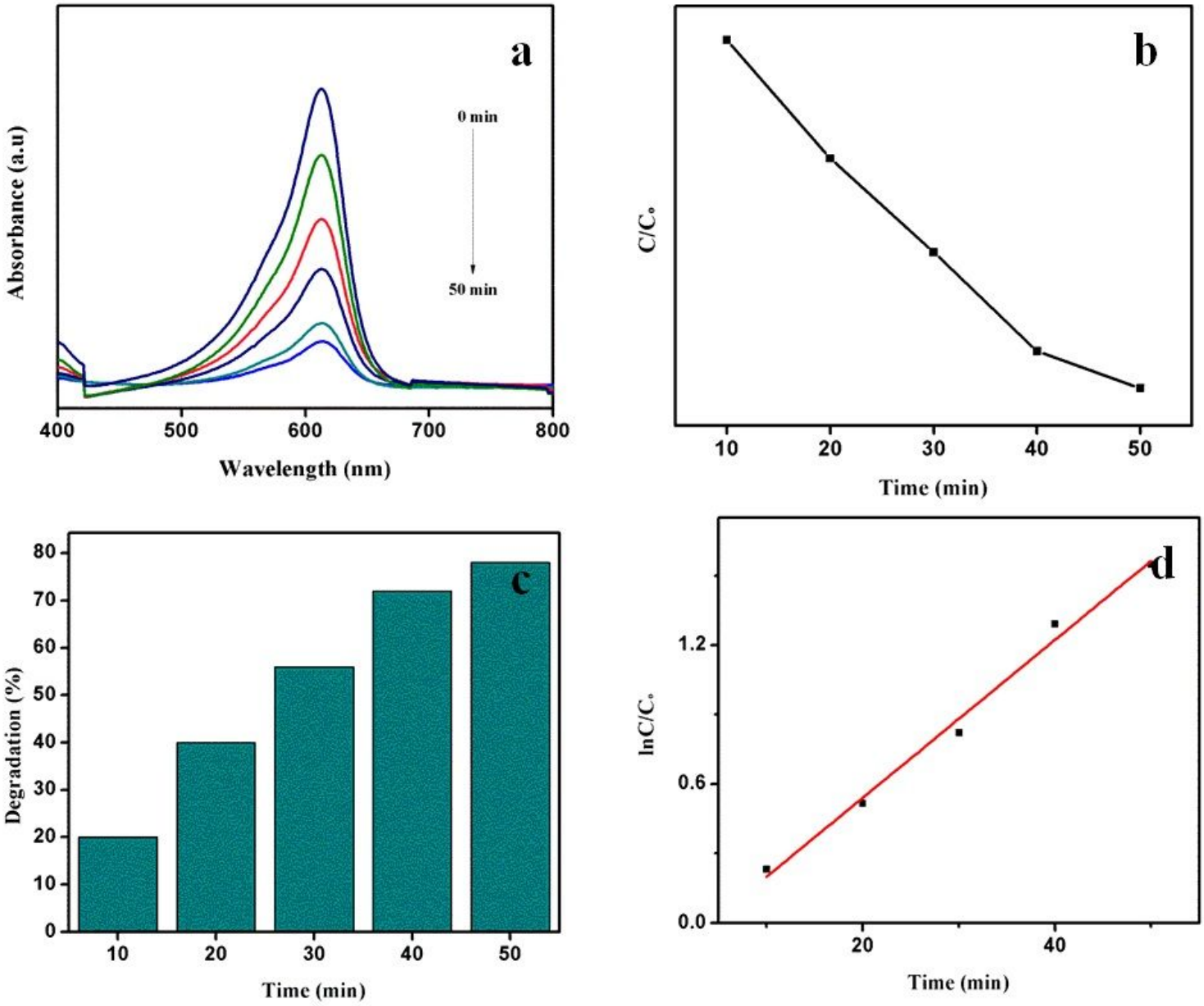

Figure 10

(a) Dye degradation (b) Concentration of C/Co (c) percentage of degradation and (d) Rate constant of IA-SnO2 nanorods.

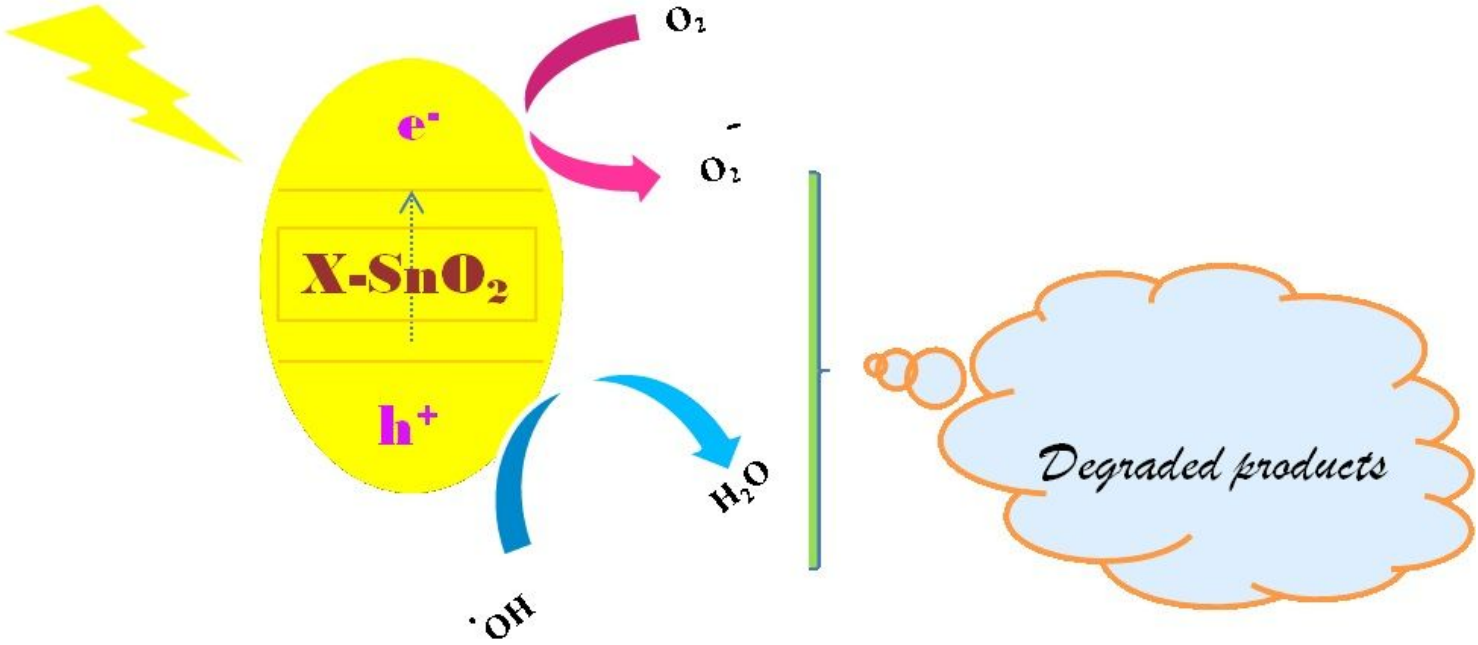

Figure 11

Degradation mechanism of X-SnO2 nanomaterials.

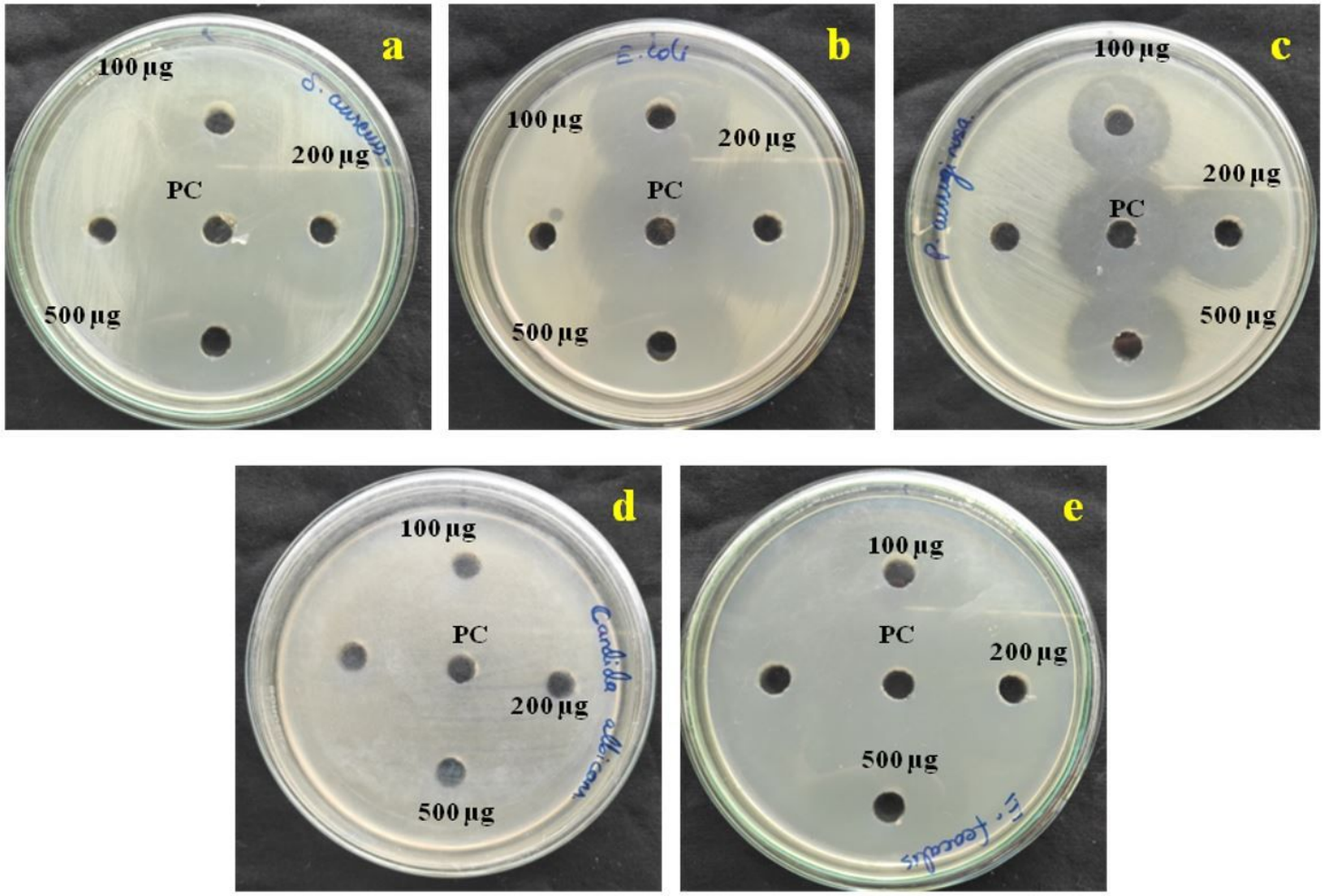

Figure 12

SnO2 nanoparticles Antibacterial and Antifungal studies: (a) S. Aureus (Gram-positive), (b) E. Coli (Gram negative) (c) P. Aeruginosa (Gram-negative) (d) C. Albicans (Antifungal) and (e) E. Faecalis bacteria (Gram-positive).